Environmental Analysis and Prediction of Lake-Effect Snow Events Downwind of Lake Ontario with Machine Learning

Carter J. Humphreys

Department of Atmospheric and Geological Sciences, State University of New York at Oswego, Oswego, New York

ABSTRACT

Prediction of lake-effect snow (LES) storms prove significant challenges for forecasters, particularly with intensity and positioning of LES bands. High-resolution mesoscale modeling improves upon the predictability of LES position and intensity, however seemingly subtle fluctuations in the atmospheric characteristics of these intense mesoscale snow bands have profound effects on the storm total precipitation. With advancements in computing, particularly with the development of machine learning and neural networks, connections between environmental conditions and LES band characteristics can be made. This research investigated band position and intensity of warning-level LES events occurring downwind of Lake Ontario in upstate New York.

A 40-case dataset of LES events from the 2015-2016 to 2019-2020 winter seasons that either had a Lake Effect Snow Warning in effect or warning-level snowfall was observed (a maximum snowfall report of at least 7” [17.8 cm] was used as a proxy for warning criteria) was constructed using NWS Storm Data and a text archive of NWS warnings. Hourly environmental conditions from various BUFKIT stations near Lake Ontario were compiled for each case. These conditions were then matched with band position (latitude and longitude coordinates) and radar reflectivity factor from nearby National Weather Service (NWS) radars. Several machine learning schemes were implemented on the dataset using scikit-learn to link environmental conditions to band position.

The results of this model demonstrate the ability for LES prediction using machine learning techniques to improve upon the guidance provided by operation forecast models and provide additional guidance for forecasters.

1. Introduction

Lake-effect snow (LES) is a localized phenomenon that occurs downwind of large bodies of water like the Great Lakes during the cold season. This mesoscale phenomenon comes in many different forms, ranging from poorly-organized snow showers that produce light snowfall (i.e. wind-parallel rolls [WPR]) to intense long lake axis-parallel (LLAP) bands that can produce snowfall rates in excess of 8 cm hr^{-1} (Steiger et al. 2013). Given the narrow width of these LES bands (on the order of a few km), small forecast placement errors of less than 20 km can result in a difference of a few cm of snowfall accumulation versus over 30 cm (Villani et al. 2017). Thus LES proves to be a significant forecasting challenge with the extreme variability and small spatial scale. Even with advancements in numerical weather prediction (NWP), significant forecast biases are common with models in band position and intensity, especially when forecasts extend further than 6 hours out (Steiger et. al 2013). An additional problem with LES prediction becomes the inland extent (IE) of the LES band, which Villani et. al (2017) showed the maximum IE of Ontario LES bands ranges from around 60 km to over 300 km downwind of the lake. LES bands can have a significant impact on society given their intense nature, causing damage to structures, vegetation, power outages and most significantly transportation (Hartmann et al. 2013).

With the growth of artificial intelligence (AI), connections between atmospheric parameters and phenomena can be made to aid forecasters and adding additional value to NWP models. AI has already shown its capabilities in improvements to meteorological phenomena through applications of machine learning to develop probabilistic quantitative precipitation forecasts from NWP output as demonstrated by Gagne et al. (2014). Additionally, Hartmann et al. (2013) used neural networks to develop seasonal prediction of LES events in Buffalo downwind of Lake Erie.

The goal of this study is to develop an application that leverages AI technology to predict band placement for LES bands downwind of Lake Ontario in New York (Fig. 1) despite the forecast challenges presented in trying to accurately predict band placement.

2. Data and Methods

a. Event Database

The event database utilized in this research was based on the database created in Humphreys and Klein (2019); which defined an case as a LES event with storm-total snowfall accumulations meeting or exceeding the Lake Effect Snow Warning/Winter Storm Warning criteria set by the National Weather Service (NWS). For the region of interest and for most of New York State, warning criteria is set at accumulations of 7 inches (17.8 cm) or greater over a period of 12 hours or less (NWS Eastern Region Supplement ERS 02-2003 to NWS Directive NWSI 10-513). For simplification, the temporal aspect of the warning criteria was ignored since solely identifying warning-level LES events was not the main focus in creating the training dataset. Events from NWS *Storm Data* categorized as LES events that occurred between the 2015-2016 and 2018-2019 winter season were fit to this criterion, resulting of in a dataset of 36 events downwind of Lake Ontario (see Table 1). Certain cases were filtered out if there was significant synoptic contamination, such as event 29 where LES band was not discernible within stratiform precipitation. Events where radar coverage was unavailable were also removed. An additional four cases from the 2019-20 season were added to the original; however, these cases (Events 37-40) were only used as testing data and were not included in the model training dataset.

b. Environmental Conditions

A similar methodology to that of Villani et al. (2017), which investigated the IE of LES downwind of Lake Ontario using six-hourly 12-km NAM analysis soundings, was used for this research. Environmental conditions were obtained from model initialization of the NOAA National Centers for Environmental Prediction's Rapid Refresh (RAP) model (Benjamin et al. 2016). BUFKIT (Mahoney and Niziol 1997) forecast soundings from the RAP at 16 different locations over and in the vicinity of Lake Ontario were utilized (Fig 2). The RAP model updates hourly, producing one hour forecasts out to 18 hours, with 13 km grid spacing and 50 vertical levels utilizing the Advanced Research WRF core. Archived RAP data was obtained from Iowa State University's Mtarchive BUFKIT Archive (Herzmann 2020). The RAP profiles were sorted into four categories: lake environment, near-lake environment, downstream environment, and upstream environment. The lake environment included the center and western Lake Ontario buoys while the near-lake environment represented locations within ~30 km of the Lake Ontario shoreline. For the downstream environment, forecast profiles were selected over the northern Finger Lakes and Tug Hill Plateau region to assess the environment where the bands would set up. The upstream environment profiles represented points near Georgian Bay, southern Ontario, and Lake Erie in order to assess the future lake environment and upstream connections with Georgian Bay. Each profile station is plotted in Fig. 2 and listed in Table 2.

In order to simplify the data processing, a BUFKIT parser was created using Python. This parser downloaded raw BUFR files from the web archive, then extracted the desired hour of the model run out of the BUFR file. A Pandas data frame was then created out of the model sounding profile and surface parameters. Quantities from the profile were then obtained by linear interpolation to get values at desired levels and exported to a comma-separated values (CSV) file.

The atmospheric variables compiled for the database (listed in Table 3) were based on similar studies: Hartmann et al. (2013) which looked at seasonal forecasting of LES using neural networks and Villani et al. (2017) using a statistical analysis for IE. Variables identified in some of the fundamental research on LES, such as Dewey (1979), Niziol et al. (1987) and Niziol et al. (1995) were also included. For the training dataset, derived quantities, such as lapse-rate and wind shear, were removed in order to simplify computations and to determine if the base (non-derivative) quantities would be sufficient enough to provide results. The training dataset variables were similar to what was used in Hartmann et al. (2013) for input values. For this research, geopotential height, air temperature, relative humidity, and u- and v-components of the wind at 925 hPa, 850 hPa, 700 hPa, and 500 hPa were used. Relative humidity at all levels were calculated using the MetPy calc Python library (May et al. 2020) routines. Occasional erroneous dewpoint values at 500 hPa resulted in relative humidity greater than 100%, which to minimize data loss, were substituted with values from the nearest level (usually between 550 hPa and 520 hPa). Additionally, satellite-derived basin-wide average water temperatures (GLERL 2019) from Lake Ontario and daily average ice cover (Kessler 2020) for Lake Ontario as well as upwind lakes (Lake Erie and Lake Huron) were included in the full dataset. Both ice cover and water temperature data were obtained from NOAA's Great Lakes Environmental Research Laboratory.

Furthermore, a separate dataset was made using only atmospheric data from the central Lake Ontario buoy (LO1) profile, i.e. average surface water temperature for Lake Ontario, and daily average ice cover from Lake Ontario, Erie, and Huron. This dataset, unlike the full dataset, included derived quantities: bulk wind shear for the 925-500 hPa, 925-850 hPa, and 925-700 hPa layers, as well as the lapse-rate from the surface water temperature between 925 hPa, 850 hPa, and 700 hPa.

c. Band Position and Intensity

Hourly band position and intensity was analyzed using reflectivity data from the WSR-88D radar in Montague, New York (KTYX); except for Event 24 where the Binghamton, New York (KBGM) WSR-88D radar provided enough coverage for analysis when KTYX was unavailable. Radar data was downloaded in hourly intervals from Amazon Web Service's Level II NEXRAD on AWS bucket (Ansari et al. 2018). Each hourly scan closest to the analysis hour was then viewed in GR2Analyst version 2.82 (http://www.grlevelx.com), and the latitude, longitude, and radar reflectivity at the 0.5 degree elevation scan was recorded along the extent of the band. The beginning of the band was marked as the point in which the band reached the shoreline (if the band was inland, the position along the shoreline was extrapolated from the start of the band). The entire length of the band was traced, with the band determined to end once it was either outside of radar coverage or the reflectivity fell below 5 dBZ. Cellular convection that was linearly organized was considered a single band. For multiple banded events, the most prominent band was traced. This process was simplified by creating a Visual Basic .NET application and utilizing the Spy++ (https://docs.microsoft.com/en-us/visualstudio/debugger/introducing-spy-increment) utility within Microsoft Visual Studio 2019 (https://visualstudio.microsoft.com). This application allowed for the band trace to be capture from the GR2Analyst window directly and export the data to a CSV file.

d. Machine Learning Schemes

The schemes available in the Python package scikit-learn (Pedregosa el al. 2011) version 0.21.3 were used to set up the machine learning application. Six different machine learning, neural networks, and regressors were utilized from this package. Initially a multi-layer perceptron (MPL) regressor, decision tree regressor (DT), and support vector regressor (SVR) were used but poor

performance in the three schemes resulted in them being dropped from the final testing. Of the original six schemes, the three best performing ones were used for final testing: a k-nearest neighbors regressor (KNN), random forest regressor (RF), and multi-linear regression (ML). The KNN regressor was run three times with instances of n=2, n=5, and n=8 neighbors, however the KNN with n=8 neighbors was dropped due to poor performance.

Two training datasets were applied: one full dataset with quantities from every point and one smaller dataset with environmental data only from LO1. Each model was trained using a 30/70 split of the database, with each instance being randomly selected. To prevent overfitting (i.e., the model memorizing the input and output) 5 K-fold cross validation splits were implemented which would stop the training if the model begins to over-train. These values were chosen at the recommendation of scikit-learn and were similar to Hartmann et al. (2013) which used a 20/80 split. Two separate versions of the four models were created with each having a different output. The first was a single output model trained using the azimuth angle between LO1 and of the band's landfalling position in order to create a simplified solution. The second group of models were multiple output regressors that were trained to produce three sets of latitude and longitude points: (1) the point where the band reaches the shoreline, (2) the midpoint of the band, and (3) the end of the LES band.

Validation of the models was done using statistical methods, including coefficient of determination (R^2) and root-mean squared error (RMSE). Additional validation was done with analysis of the predictions with radar data using Py-ART (Helmus and Collis 2016). For azimuth angle predictions, a line was plotted from LO1 for the predicted angle along a 100 km radial. For the model predictions of exact band positions, a line was plotted with the latitude and longitude coordinates for the band start (i.e., at the shoreline), midpoint, and end point.

3. Results

a. Database Statistics

The accuracy of the model in predicting LES band placement is tied to how well events correlate with the atmospheric conditions the model has been trained with. The distribution of each atmospheric and lake variable used is shown in Fig. 3.

I. BAND PLACEMENT

In total, 1145 hourly band positions were identified over the 4-year period, shown in Fig. 4. A maximum in LES band frequency expectedly occurs over the Tug Hill Plateau region, directly downwind of the lake. Relative band frequency tends to drop off outside of immediate downwind of Lake Ontario (Jefferson, Lewis, and Oswego Counties), but does extend into the western Adirondacks and northern Central New York.

II. WATER TEMPERATURE AND ICE COVER

The 25th and 75th percentile values of the average Lake Ontario surface water temperature were 2.82 °C and 6.14 °C while the 25th and 75th percentile values of the daily average ice cover were 0.07% and 8.16%. Greater variability in ice cover was found in upstream lakes as the 25th and 75th percentile values for Lake Huron (Lake Erie) were 0.35% and 33.50% (0.00% and 46.79%), as expected given the shallow nature of these bodies compared to Lake Ontario (Assel 2005).

III. GEOPOTENTIAL HEIGHT

Looking at the environmental conditions for the LO1 profile, the interquartile range for 850 hPa geopotential height was 1338 m to 1410 m, and 500 hPa height was 5186 m to 5321 m. These ranges for 850 hPa and 500 hPa geopotential heights correlated well with Hitchcock (2019)

for both minor and major LES events downwind of Lake Ontario, which showed a mean geopotential height of 5200 m over Lake Ontario during the middle of an event.

IV. INSTABILITY

The lapse rates for layers between the lake surface and 925 hPa, 850 hPa, and 700 hPa level were also computed. The 25th and 75th percentile ranges for the layer from the surface to 925 hPa were 16.29 °C/km to 22.64 °C/km, yielding a super-adiabatic lapse rate. For the surface to 850 hPa layer, the 25th and 75th percentile values were 8.53 °C/km and 12.14 °C/km, indicating a conditionally unstable environment. Finally, the surface to 700 hPa-layer lapse rates ranged between 4.12 °C/km and 5.93 °C/km, revealing stable to weak instability in the mid-levels. This provides evidence that for half of the events the greatest instability was confined to the lower boundary layer, as expected given the shallow nature of the convection in LES. Lapse rates also weakened near the 700 mb layer likely as a result of the transition (capping inversion) between the well mixed dry-neutral boundary layer and the free atmosphere above.

V. STEERING LAYER FLOW

Through the steering layer, which was defined by Niziol (1987) as the wind direction from the first 50 hPa through 700 hPa, winds within the steering layer were characterized by a positive u-component (i.e., westerly wind) in just about all of the cases (Fig. 3). The u-component 25th and 75th percentile values were around 15.03 kts and 26.08 kts at 925 hPa and 19.38 kts and 31.11 kts for 850 hPa. For the v-component of the wind, values were either positive (i.e., southerly) or slightly negative (i.e., northerly). The 25th and 75th percentile values of the v-component wind were -1.56 kts and 13.38 kts at 925 hPa. Going up in the atmosphere to 850 hPa, the wind tended to have slightly less of a southerly component and more of a northerly component as evident by the interquartile range of -2.42 kts and 12.69 kts. At the 700 hPa surface, similar but stronger flow

(both u- and v-components) occurred. The interquartile range for the u-component at 700 hPa was 25.1 kts and 38.39 kts showing strong westerly flow at the top or above the boundary. For the v-component, the interquartile range showed a weak northerly component aloft at -3.34 kts to strong southerly flow at 17.64 kts. These ranges through the steering layer demonstrated that for most of the cases, a strong westerly or southwesterly wind is common for the events. These results imply that many cases likely had LLAP bands as the primary band type given the domain flow oriented parallel to the long axis of Lake Ontario.

VI. WIND SHEAR

Bulk shear over the 925-850 hPa, 925-700 hPa, and 925-500 hPa increased with the increasing height and thickness of the layer. The bulk shear values at the 25^{th} and 75^{th} percentile for the 925-850 hPa layer were respectively 10.76 kts and 37.29 kts, 9.67 kts and 38.04 kts between 925-700 hPa, and 15.15 kts and 47.45 kts between 925-500 hPa.

b. Azimuthal Angle Model Performance

I. FULL ENVIRONMENTAL DATABASE MODEL

For the azimuthal angle prediction model, the best performance comes from the KKN (n=2) model, with a mean cross-validation (CV) score of 0.710 ± 0.048 (Fig. 5c) at the 95% confidence interval. This was followed by the RF at 0.626 ± 0.029 (Fig. 5e) , KNN (n=5) at 0.628 ± 0.080 (Fig. 5d), and MLR at 0.468 ± 0.081 (Fig. 5f). The overall distribution of the algorithms score can be seen in Fig. 5a. Figure 5b shows the R^2 value for each algorithm, this showed similar results to the mean CV score in terms of order, but with slightly higher skill. The KNN (n=2) R^2 was 0.781 with an RMSE of 10.574°, RF with an R^2 of 0.736 and RMSE of 11.604°, the KNN (n=5) with an

R^2 of 0.714 and RMSE of 12.082°, and finally the MLR with an R^2 of 0.559 and an a RMSE of 15.006°.

II. LO1 ENVIRONMENTAL DATABASE MODEL

Using the LO1 environmental database, the best performance again comes from the KKN (n=2) model, with a mean CV score of 0.706 ± 0.041 (Fig. 6c) at the 95% confidence interval. Similar to the full environmental database, model skill was followed by the RF model with 0.611 ± 0.048 (Fig. 6e), KNN (n=5) with a skill of 0.599 ± 0.065 (Fig. 6d), and the MLR at 0.376 ± 0.032 (Fig. 6f). The overall distribution of the algorithms score can be seen in Fig. 6a. Looking at the predictability of the models, the R^2 (Fig. 6b) followed a similar order with the KNN (n=2) R^2 at 0.772 with an RMSE of 10.784°, then the RF R^2 at 0.733 and RMSE at 11.684°, KNN(n=5) R^2 of 0.705 and RMSE of 12.264°, concluding with the MLR with an R^2 of 0.518 and RMSE of 15.681°.

c. Band Orientation Model Performance

I. FULL ENVIRONMENTAL DATABASE MODEL

Like the model skill with the LES band azimuth angle algorithms, the best performance comes from the KKN (n=2) model, with a mean CV score of 0.754 ± 0.031 at the 95% confidence interval. This was followed by the KNN (n=5) at 0.683 ± 0.033, RF at 0.668 ± 0.026, and MLR at 0.538 ± 0.033. The overall distribution of the algorithms score can be seen in Fig. 7a. Figure 7b shows the R^2 for each algorithm, this again showed similar results to the mean CV score in terms of order, but with slightly higher skill. The KNN (n=2) R^2 was 0.813 with an RMSE of 0.187°, KNN (n=5) with an R^2 of 0.764 and RMSE of 0.212°, RF with an R^2 of 0.720 and RMSE of 0.239°, and lastly the MLR with an R^2 of 0.614 and an a RMSE of 0.269°.

The KNN (n=2) again yielded the best performance overall, with a mean CV score at the 95% confidence interval at 0.730 ± 0.043. KNN (n=2) was followed by KNN (n=5) at 0.650 ± 0.050, RF 0.636 ± 0.042, and finally the MLR 0.440 ± 0.035. The overall distribution of the algorithms score can be seen in Fig. 8a. Measuring model skill and predictability with R^2 (Fig. 8b) shows a similar order of performance but with higher skill. KNN (n=2) model had an R^2 of 0.796 with an RMSE of 0.202°, followed by the KNN (n=5) at 0.750 for an R^2 and 0.221° for RMSE, RF with an R^2 of 0.737 and RMSE at 0.228°, then at the end of the list the MLR with an R^2 of 0.494 and an RMSE of 0.319°.

4. Summary and Conclusions

Analysis of the model training yielded that the KKN (n=2) regressor was the best algorithm for creating a viable model in LES prediction. The KKN (n=2) outperformed the other algorithms (KNN n=5, RF, and MLR) when compared using all datasets and model outputs. Comparing the models using the different datasets yielded a similar result in terms of skill for prediction of band orientation and angle. In direct analysis of randomly selected output, no significant advantage was found for using one database over the other, further examination is needed to determine why this is the case. An example of the output showing better performance with complete lake environment database is shown in Fig. 9, with the opposite being shown in Fig 10.

a. Model Assumptions

There are some assumptions that will be required in order to accurately interpret the output from these models that result from the input dataset or algorithm computations.

I. USE IN UNFAVORABLE LES CONDITIONS

Data fed into the model is assumed to have LES occurring, as no training was done with conditions that were unfavorable for LES occurring. Future development into determining if LES would be occurring under a given set of conditions would be necessary to alleviate this assumption.

II. RAP MODEL BIAS

Given that training was performed using the RAP initialization data, any biases that develop within the RAP forecast data could influence the position data. However, given the course 13 km spatial resolution and broad data points, the likelihood of any anomalous values should be minimal. This is in contrast with high resolution models that can simulate more localized atmospheric conditions, which may result in local noise and possibly skew results.

III. AZIMUTHAL ANGLE INDICATOR

With the azimuthal angle prediction, the assumption must be made that the band exists at the shoreline. This was done in order to keep the output consistent for the model and alleviate the need for range prediction. This can result in LES band azimuthal angle values that point to a shoreline location, while the actual LES band may not be present at this location but extend further inland. The line indication from LO1 is also not a representation of flow over the lake, even though it may be aligned with the band. The actual band orientation may differ greatly from the indication, especially for events whose flow features a strong southerly or northerly component (Fig. 11).

IV. BAND WIDTH

None for the algorithm used in this study had band width included within the dataset. An assumption of band width would need to be made by the user interpreting the output of the models. This becomes especially true during WPR events, where the width of the band can be much greater than that of LLAP bands. For WPR events, the model indication is for the center and most intense

band of the WPRs (Fig. 12). This condition will also apply to events with dual LLAP bands, where the position indicator and orientation will be for the most intense LLAP band (Fig. 13).

V. INLAND EXTENT

As previously shown in Fig. 4, the hourly band positions identified over the 4-year period tend to extend inland into the western Adirondacks and northern Central New York. This termination point is detectable for most LES bands as this distance lies about 100 to 120 km inland from the shore. However, this inland distance correlates with a beam height of the 0.5° tilt from KTYX radar exceeding 2 km AGL (Fig. 14) as KTYX sits 0.52 km above Lake Ontario. This may have resulted in some early termination of the LES given their shallow convective nature and tendency for the radar beam to overshoot the LES band as discussed in Brown et. al (2007). Further analysis of the nearby radars Binghamton, NY (KBGM), Albany, NY (KENX), and Burlington, VT (KCXX) radars or satellite data would be needed to assess this.

b. Future Work

The models presented in this research are by no means a perfect solution to solve the forecasting challenge presented by LES events, by rather a proof of concept for further development to build off. Further development relating band position and intensity to snowfall could prove valuable for operational forecasters predicting storm-total snowfall accumulations. Additionally, the use of band position data and machine learning to bias correct high-resolution operational model guidance (e.g., HRRR, NAM Nest) could potentially be useful to forecasters.

The code and example out used in this research is available via GitHub repository github.com/HumphreysCarter/LES-Machine-Learning. Output from the machine learning model can be viewed at carterhumphreys.com/research/les-band-position.

Lake Ontario Lake Effect Snow (LES) Events (October 2015 – February 2020)

EVENT ID	EVENT BEGIN	EVENT END	DURATION [HRS]
1	2015-10-17 10:00	2015-10-18 18:00	32
2	2015-12-18 09:00	2015-12-20 05:00	44
3	2015-12-31 12:00	2016-01-02 11:00	47
4	2016-01-11 03:00	2016-01-12 07:00	28
5	2016-01-13 18:00	2016-01-14 22:00	28
6	2016-01-18 06:00	2016-01-19 11:00	29
7	2016-01-27 07:00	2016-01-27 13:00	6
8	2016-02-10 17:00	2016-02-11 11:00	18
9	2016-02-12 19:00	2016-02-13 12:00	17
10	2016-11-22 10:00	2016-11-22 16:00	6
11	2016-12-08 03:00	2016-12-09 07:00	28
12	2016-12-10 14:00	2016-12-11 20:00	30
13	2016-12-14 00:00	2016-12-15 14:00	38
14	2016-12-29 18:00	2016-12-31 11:00	41
15	2017-01-04 22:00	2017-01-07 12:00	62
16	2017-01-27 02:00	2017-01-30 05:00	75
17	2017-02-01 09:00	2017-02-04 23:00	86
18	2017-02-10 01:00	2017-02-10 15:00	14
19	2017-11-19 18:00	2017-11-20 22:00	28
20	2017-12-06 09:00	2017-12-08 17:00	56
21	2017-12-10 07:00	2017-12-11 10:00	27
22	2017-12-16 00:00	2017-12-16 18:00	18
23	2017-12-25 15:00	2017-12-28 01:00	58
24	2017-12-30 18:00	2017-12-31 00:00	6
25	2018-01-02 18:00	2018-01-03 16:00	22
26	2018-01-04 00:00	2018-01-06 23:00	71
27	2018-02-02 06:00	2018-02-04 00:00	42
28	2018-02-08 08:00	2018-02-09 17:00	33
29	2018-11-27 12:00	2018-11-29 09:00	45
30	2018-12-06 03:00	2018-12-07 02:00	23
31	2019-01-09 17:00	2019-01-10 03:00	10
32	2019-01-25 00:00	2019-01-26 21:00	45
33	2019-02-08 15:00	2019-02-09 18:00	27
34	2019-02-14 00:00	2019-02-14 15:00	15
35	2019-03-04 21:00	2019-03-07 08:00	59
36	2019-03-31 21:00	2019-04-01 10:00	13
37	2019-12-18 02:00	2019-12-19 03:00	25
38	2020-01-06 13:00	2020-01-07 02:00	13
39	2020-02-19 23:00	2020-02-20 13:00	14
40	2020-02-27 15:00	2020-02-29 06:00	39

Table 1. List of the 40 events used in the dataset. Events 1-36 from Humphreys and Klein (2019).

Available RAP BUFKIT Profiles

LAKE ENVIRONMENT	NEAR-LAKE ENVIRONMENT	DOWNSTREAM ENVIRONMENT	UPSTREAM ENVIRONMENT
LO1 (C. Lake Ontario Buoy)	CYYZ (Toronto, Canada)	KSYR (Syracuse, NY)	CYHM (Hamilton, Canada)
LO2 (W. Lake Ontario Buoy)	KART (Watertown, NY)	KUCA (Utica, NY)	CYQA (Muskoka, Canada)
	KROC (Rochester, NY)	RME (Rome, NY)	GNB (Georgian Bay Buoy)
	KIAG (Niagara Falls, NY)	RME (Rome, NY)	LE3 (E. Lake Erie Buoy)
	CYPQ (Peterborough, Canada)	OGS (Ogdensburg, NY)	
		GTB (Fort Drum, NY)	

Table 2. List of RAP profiles used in the environmental database.

Environmental Variables Used in Dataset

SOURCE	VARIABLE	LEVEL
RAP Initialization	Air Temperature	925 hPa
		850 hPa
		700 hPa
		500 hPa
RAP Initialization	Relative Humidity	925 hPa
		850 hPa
		700 hPa
		500 hPa
RAP Initialization	Wind U-Component	925 hPa
		850 hPa
		700 hPa
		500 hPa
RAP Initialization	Wind V-Component	925 hPa
		850 hPa
		700 hPa
		500 hPa
RAP Initialization	Bulk Wind Shear	925-850 hPa
		925-700 hPa
		925-500 hPa
RAP Initialization	Lapse Rate	T_{water}-$T_{925\ hPa}$
		T_{water}-$T_{850\ hPa}$
		T_{water}-$T_{700\ hPa}$
GLERL	Average Daily Water Temperature	Lake Ontario
GLERL	Average Daily Ice Cover	Lake Ontario
		Lake Erie
		Lake Huron

Table 3. List of variables used in the environmental database.

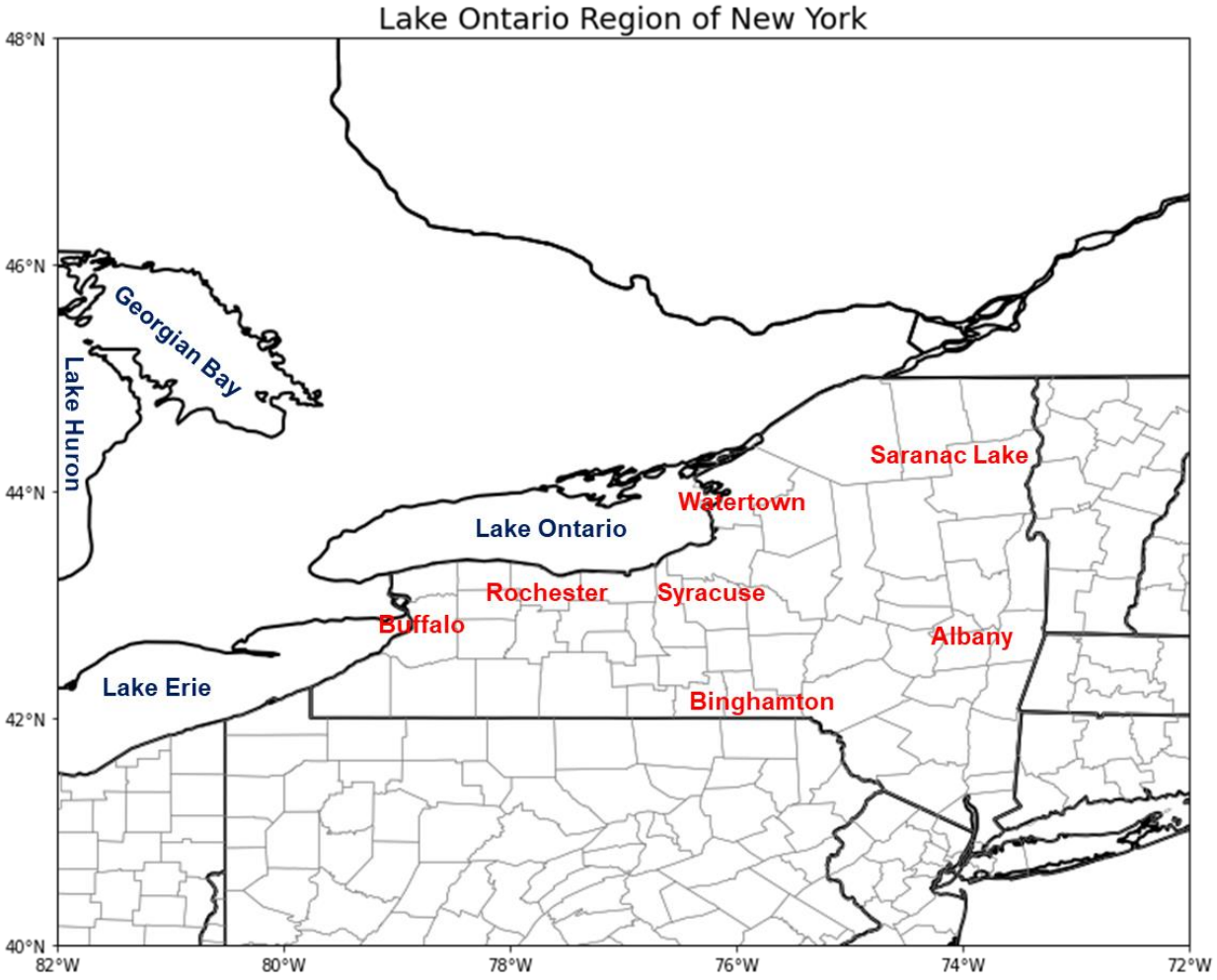

Figure 1. Map of the Lake Ontario region of New York State. Lakes are labeled in blue and select cities labeled in red.

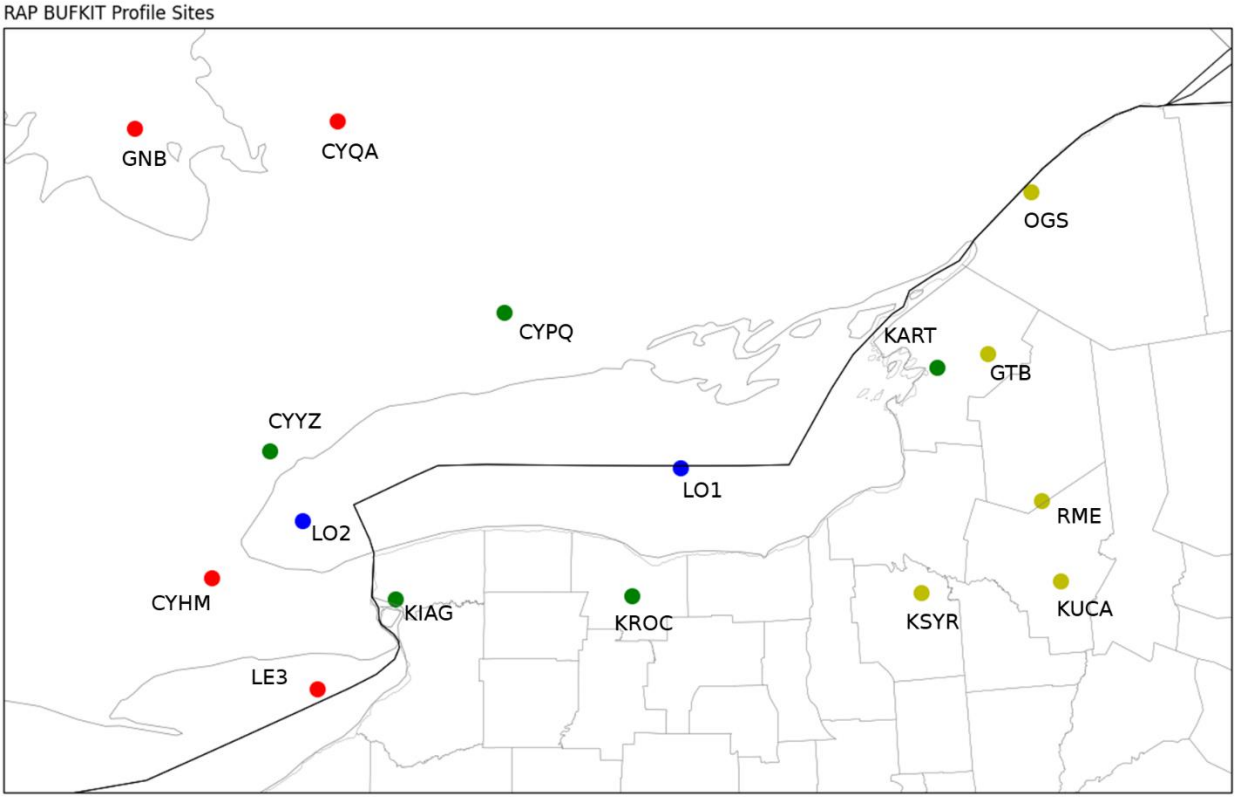

Figure 2. Map of available RAP BUKFKIT profile locations. Red markers indicate upwind environment, green indicate near-lake environment, blue represent lake environment, and yellow represent the downwind environment.

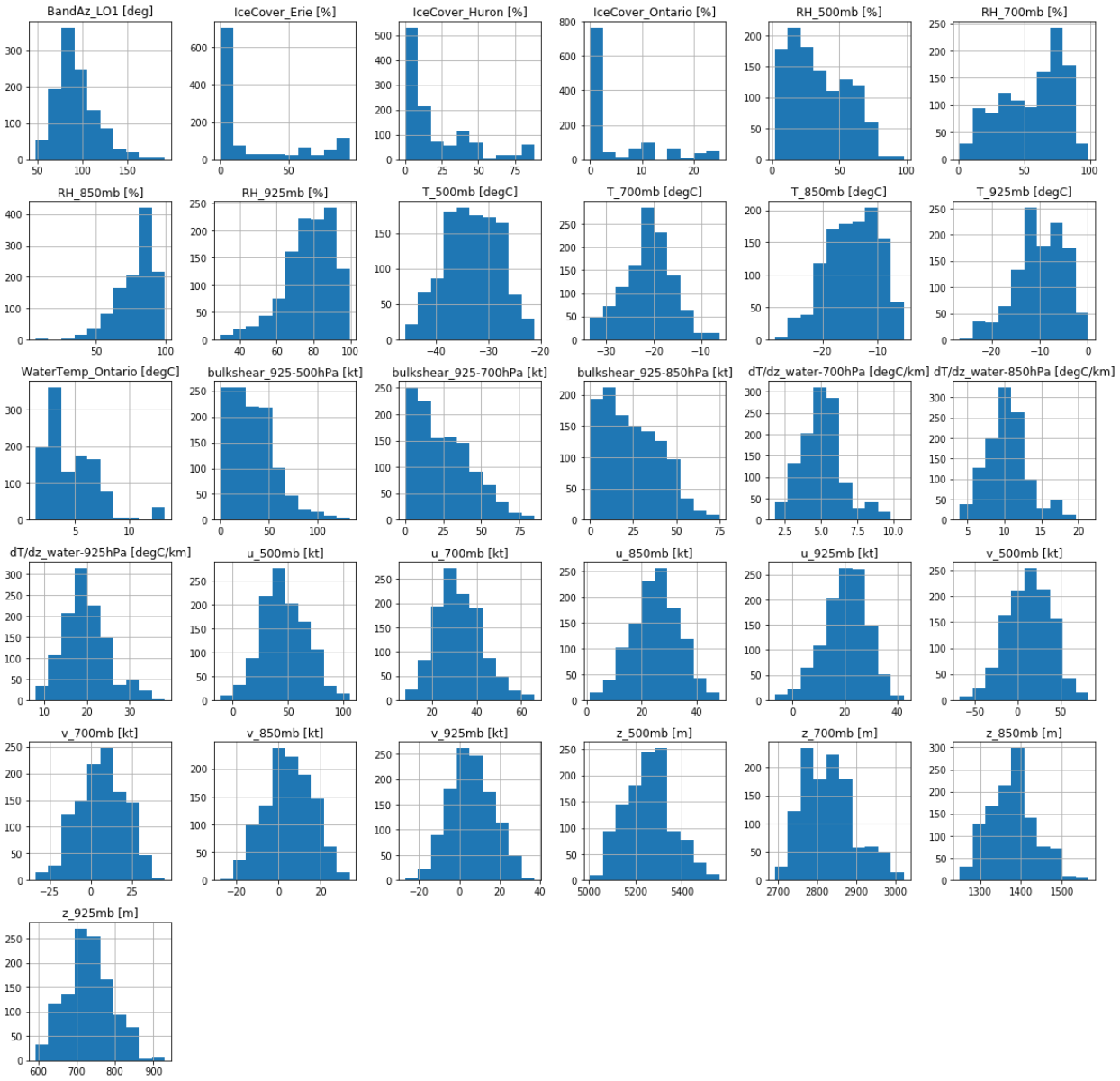

Figure 3. Histogram of the environmental variables from RAP initialization over Central Lake Ontario.

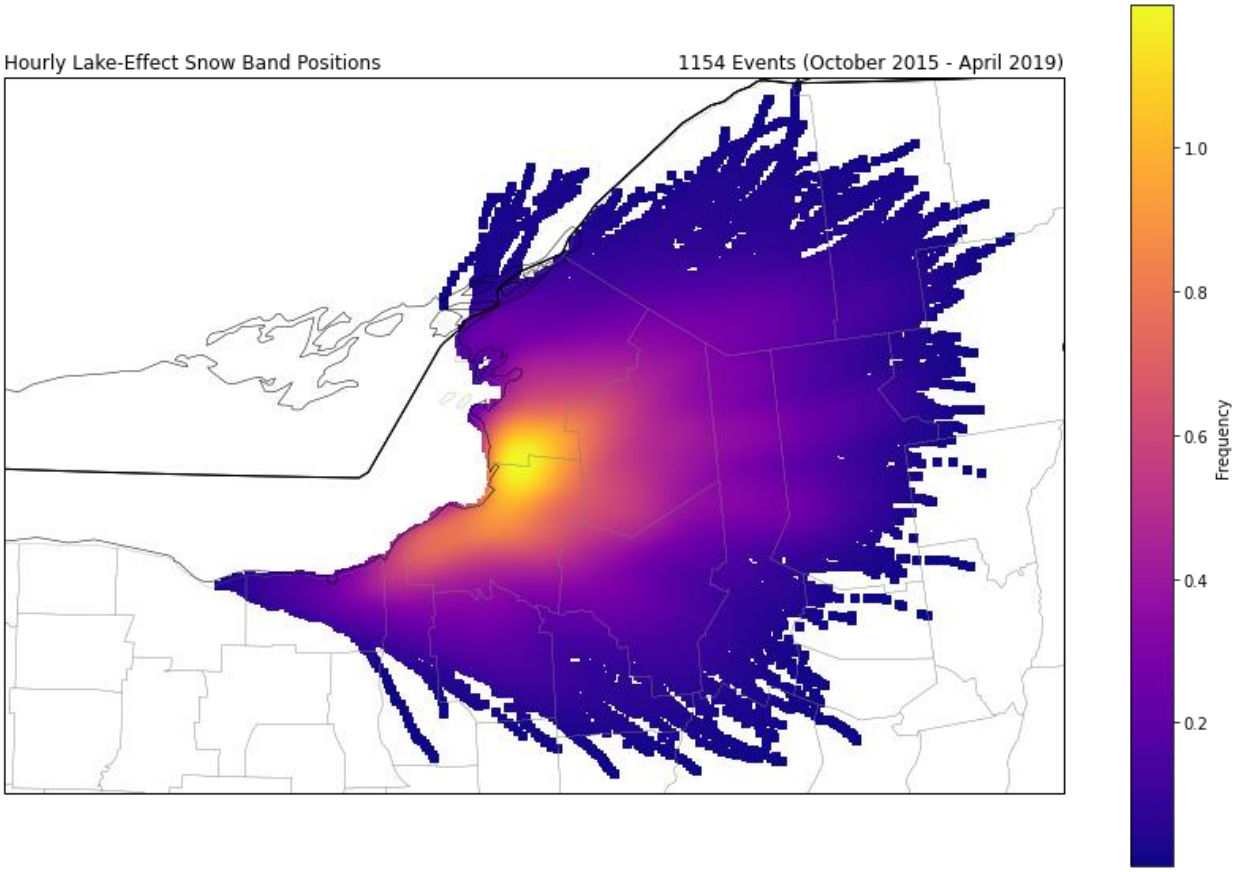

Figure 4. Spacial analysis plot of the 1145 hourly band positions that were analyzed over the 4-year period from October 2015 to April 2019, colored with respect to frequency.

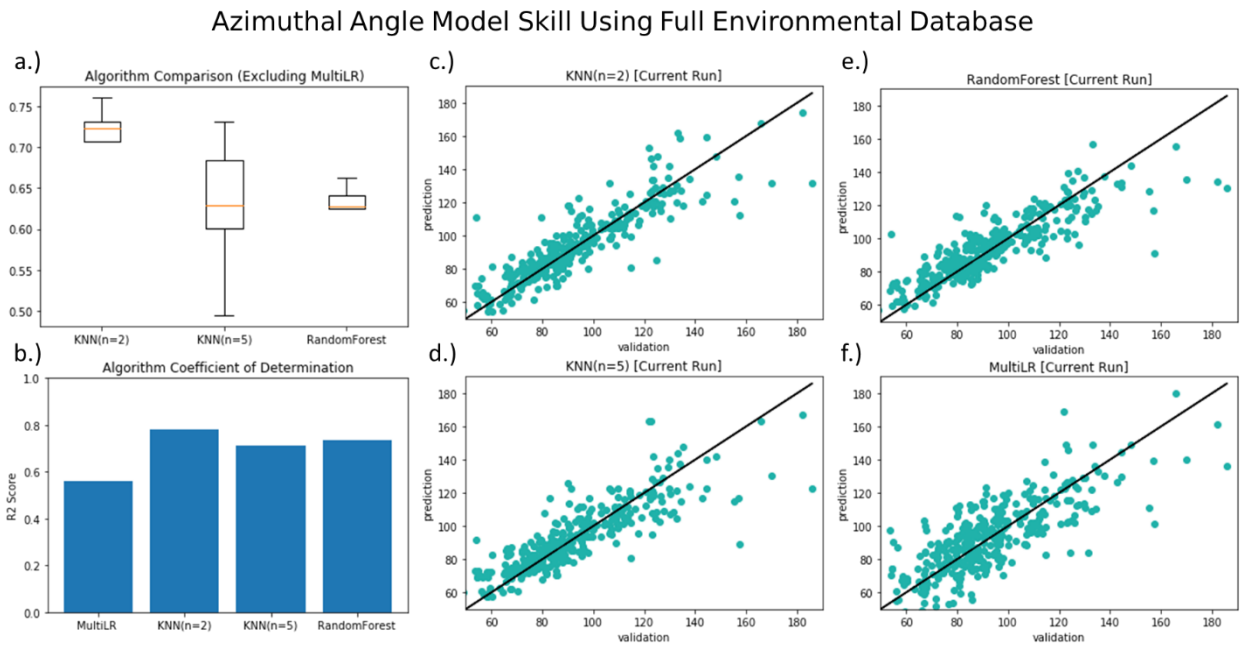

Figure 5. Model skill for the azimuthal angle model using the full environmental database. (a) box and whisker plot of average model skill at 95% confidence interval, (b) algorithm coefficient of determination (R^2), (c) validation vs prediction for K-Nearest Neighbors with 2 neighbors, (d) validation vs prediction for K-Nearest Neighbors with 5 neighbors, (e) validation vs prediction for Random Forest, (f) validation vs prediction for multi-linear regression.

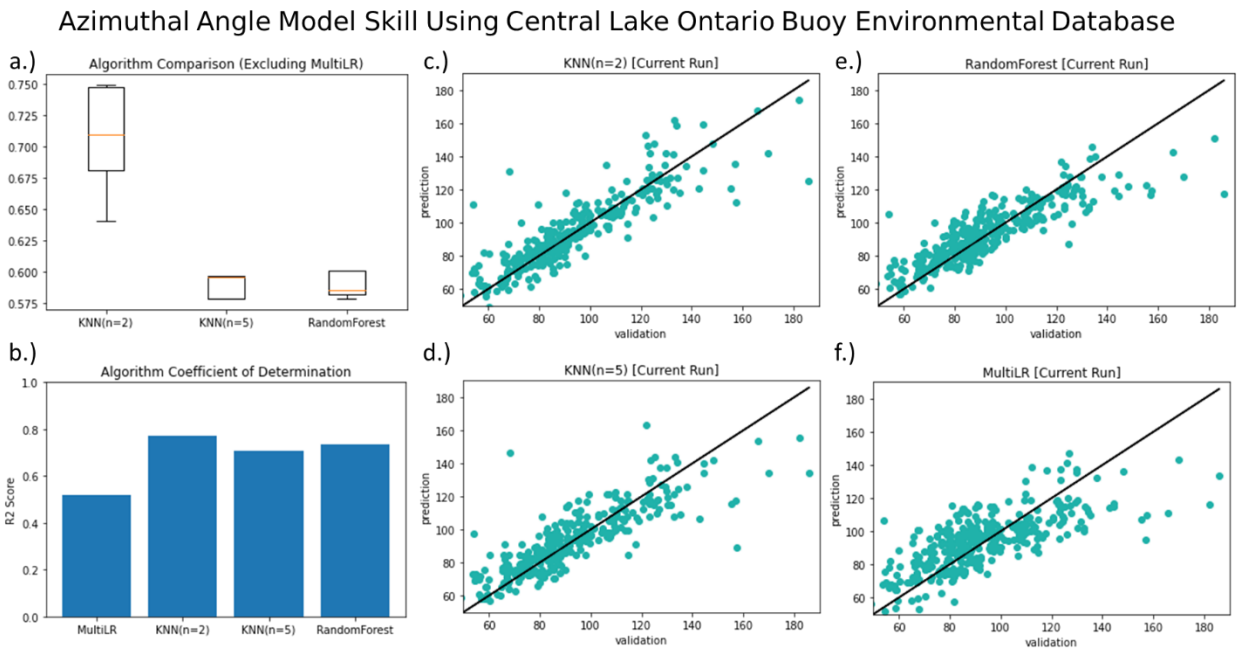

Figure 6. Model skill for the azimuthal angle model using the central Lake Ontario buoy environmental database. (a) box and whisker plot of average model skill at 95% confidence interval, (b) algorithm coefficient of determination (R^2), (c) validation vs prediction for K-Nearest Neighbors with 2 neighbors, (d) validation vs prediction for K-Nearest Neighbors with 5 neighbors, (e) validation vs prediction for Random Forest, (f) validation vs prediction for multi-linear regression.

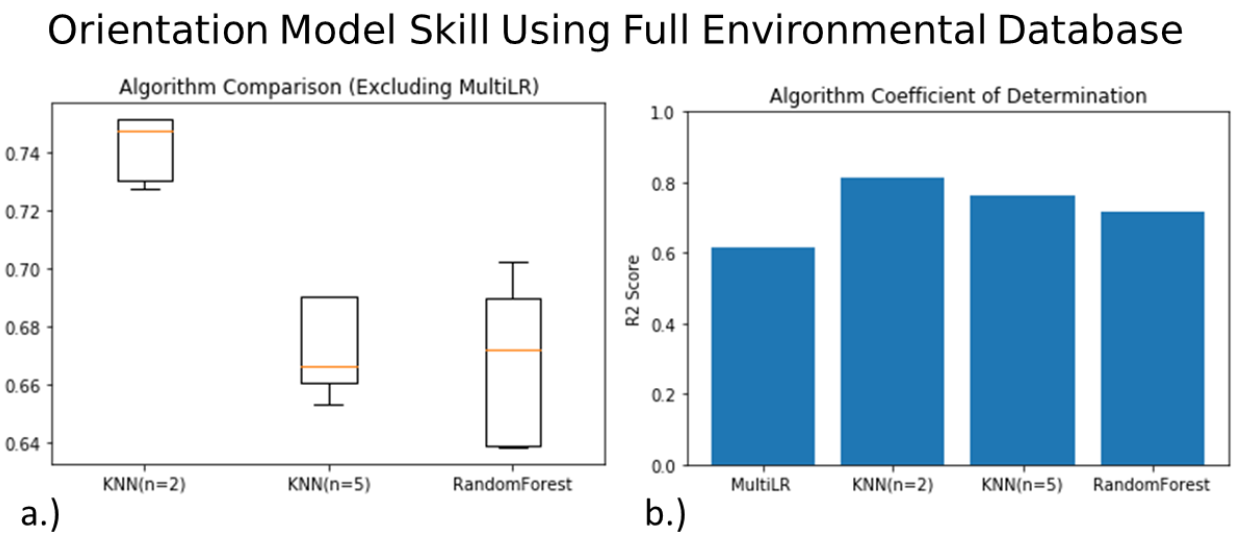

Figure 7. Model skill for lake-effect snow band orientation model using the full environmental database. (a) box and whisker plot of average model skill at 95% confidence interval, (b) algorithm coefficient of determination (R^2).

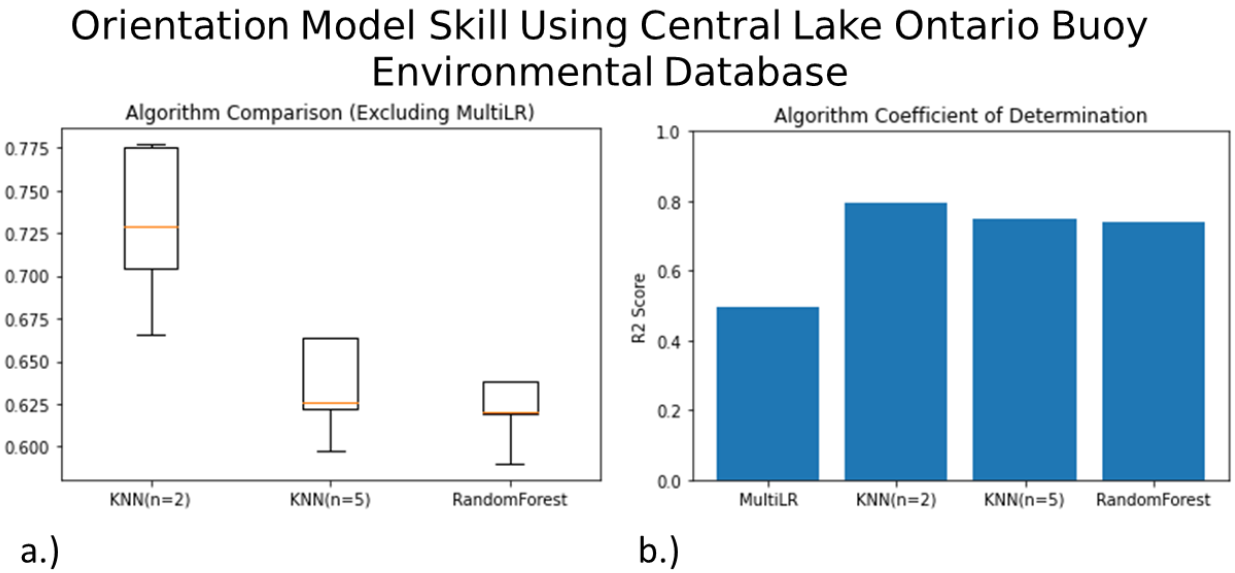

Figure 8. Model skill for lake-effect snow band orientation model using the central Lake Ontario buoy environmental database. (a) box and whisker plot of average model skill at 95% confidence interval, (b) algorithm coefficient of determination (R^2).

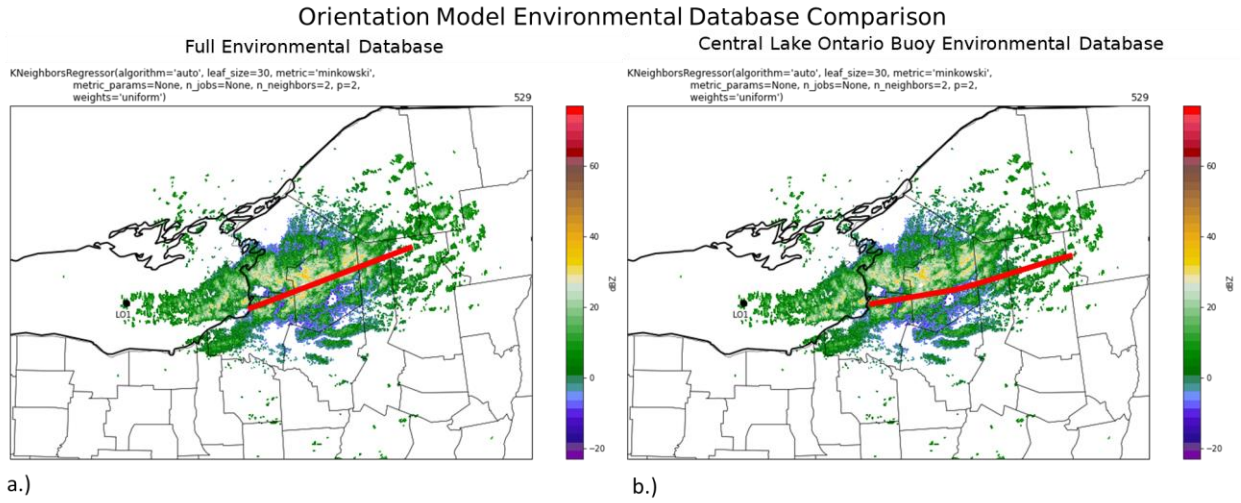

Figure 9. Comparison of lake-effect band orientation prediction using (a) full database and (b) central Lake Ontario database . The predicted band is indicated by the red line.

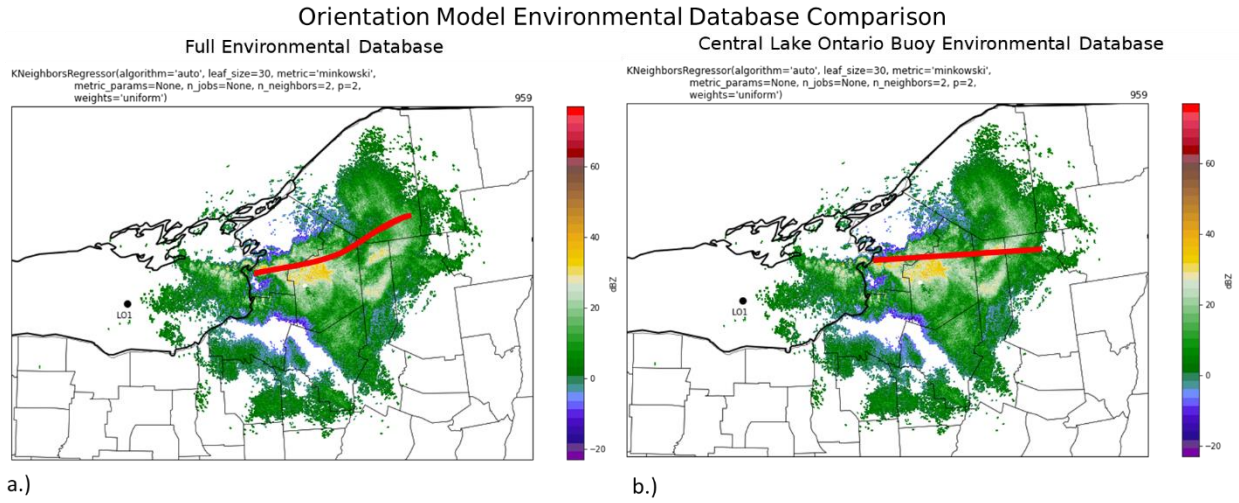

Figure 10. Comparison of lake-effect band orientation prediction using (a) full database and (b) central Lake Ontario database. The predicted band is indicated by the red line.

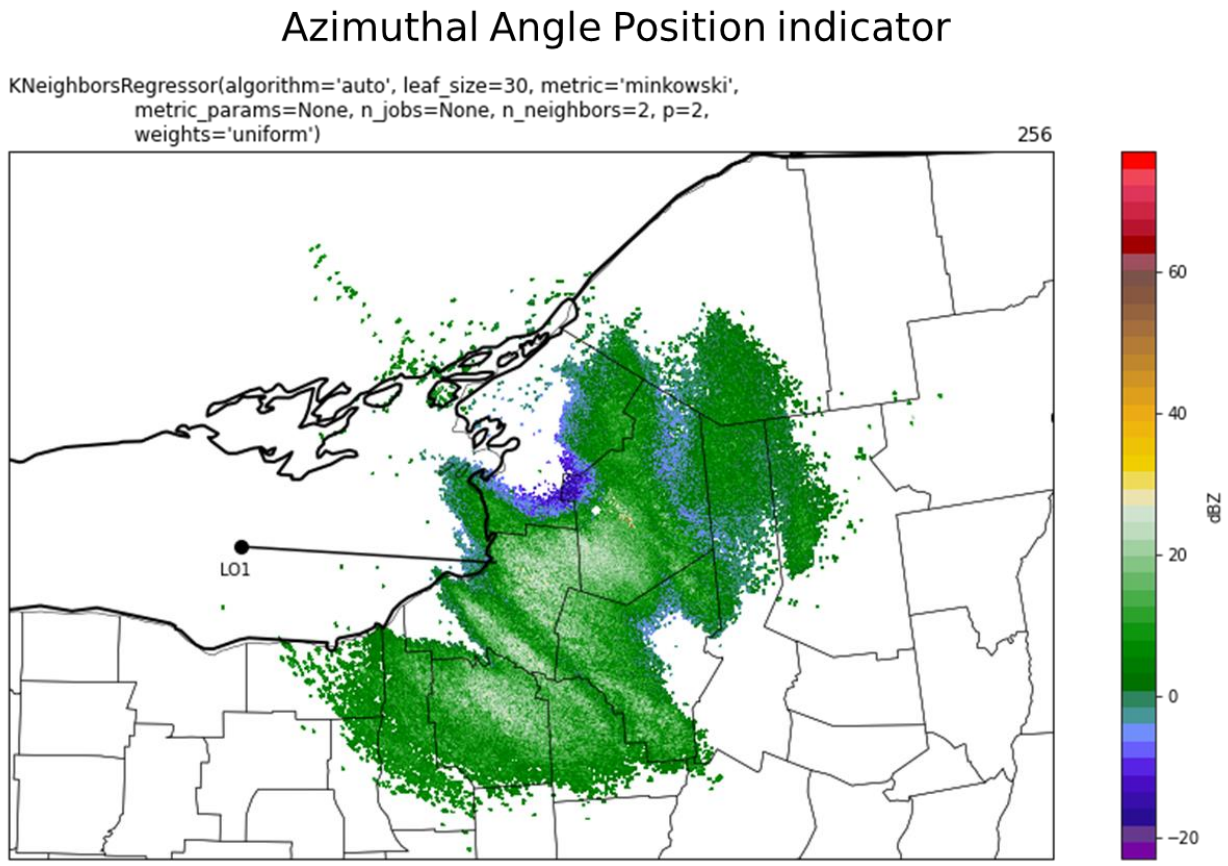

Figure 11. Azimuth angle model position indicator with bands resulting from northwest flow.

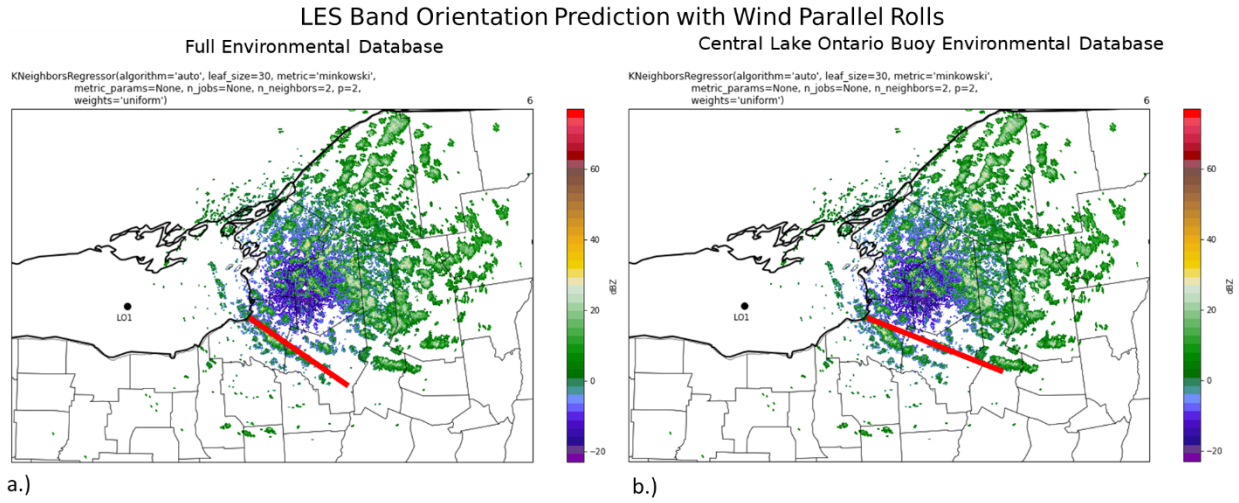

Figure 12. Comparison of lake-effect band orientation prediction using (a) full database and (b) central Lake Ontario database with wind parallel rolls. The predicted band is indicated by the red line.

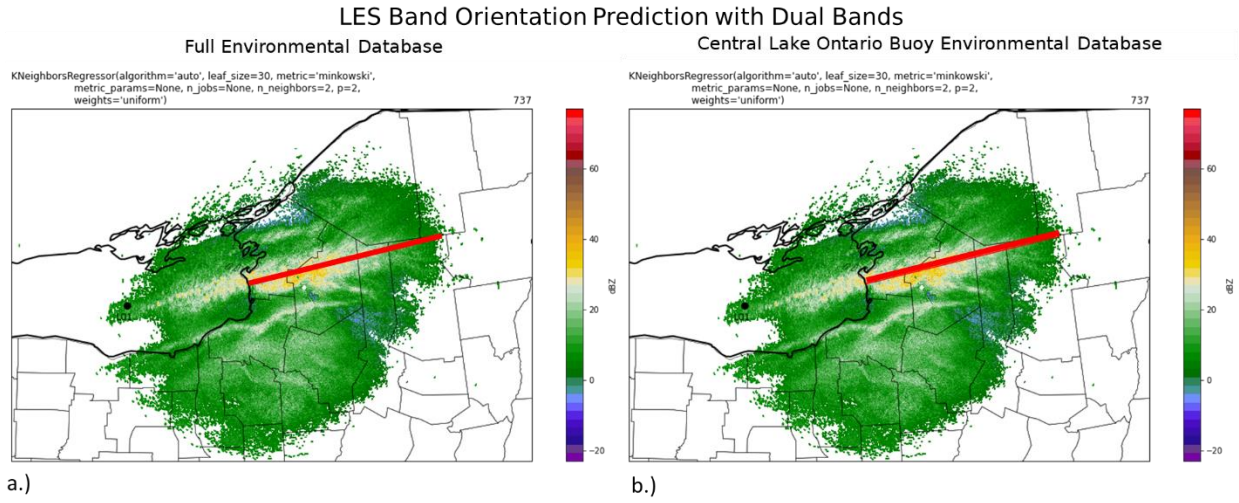

Figure 13. Comparison of lake-effect band orientation prediction using (a) full database and (b) central Lake Ontario database with dual bands. The predicted band is indicated by the red line.

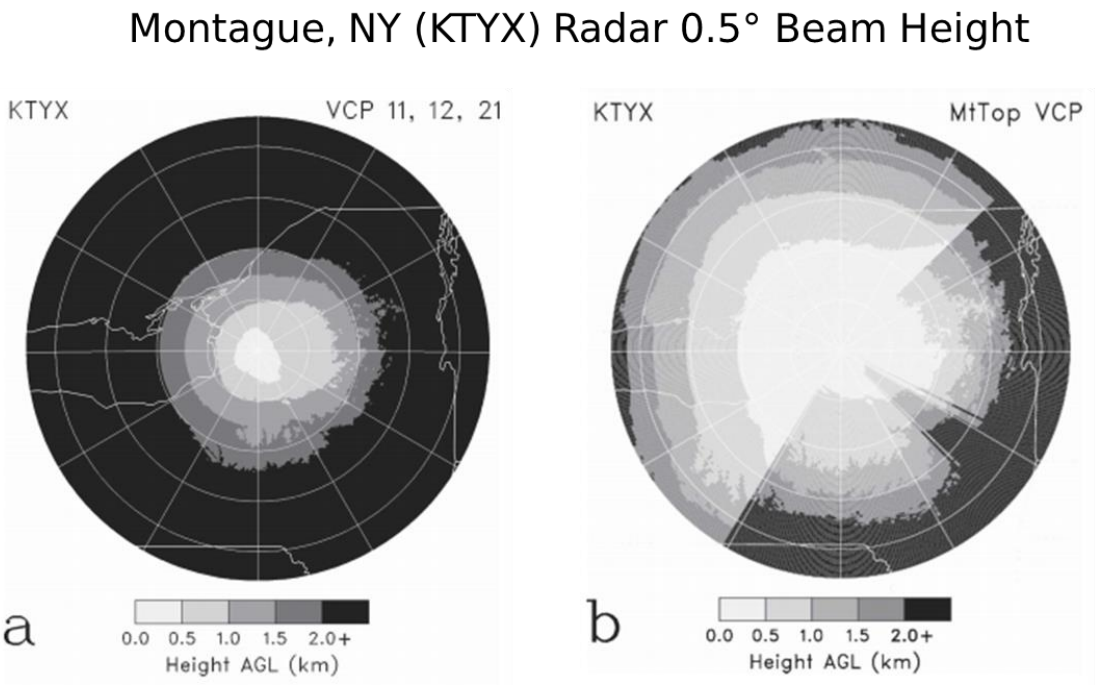

Figure 14. Heights of lowest elevation angles above Lake Ontario and adjacent terrain for KTYX using (a) VCPs 11, 12, and 21 (0.5°) and (b) the mountaintop VCP (-0.4°, 0.0°, 0.4°) . The black area is more than 2 km above the surface. Range rings are at 50-km intervals. Figure reproduced from Brown et al. (2007).

REFERENCES

Ansari, S., and Coauthors, 2018: Unlocking the potential of NEXRAD data through NOAA's Big Data Partnership. *Bull. Amer. Meteor. Soc.*, **99**, 189–204.

Assel, R. A., 2005: Great Lakes Weekly Ice Cover Statistics. NOAA Technical Memorandum GLERL 133, 27 pp.

Benjamin, S. G., and Coauthors, 2016: A North American hourly assimilation and model forecast cycle: The Rapid Refresh. *Mon. Wea. Rev.*, **144**, 1669–1694.

Brown, A. R., T. A. Niziol, N. R. Donaldson, P. I. Joe, V. T. Wood, 2007: Improved Detection Using Negative Elevation Angles for Mountaintop WSR-88Ds. Part III: Simulations of Shallow Convective Activity over and around Lake Ontario. *Mon. Wea. Rev.*, **119**, 2323–2332.

Dewey, K. F., 1979: Lake Eire Induced Mesosystems – An Operational Forecast Model. *Mon. Wea. Rev.*, **107**, 421–425.

Gagne, D. J., II, A. McGovern, and M. Xue, 2014: Machine learning enhancement of storm-scale ensemble probabilistic quantitative precipitation forecasts. *Wea. Forecasting*, **29**, 1024–1043.

Gibson Ridge Software, 2020: GR2Analyst. Version 2.82, Gibson Ridge Software, LLC, Accessed 04 March 2020.

GLERL, 2019: Average GLSEA Surface Water Temperature Data. NOAA Great Lakes Environmental Research Laboratory, accessed 17 April 2020, https://coastwatch.glerl.noaa.gov/statistic.

Hartmann, H., J. Livingston, and M.G. Stapleton, 2013: Seasonal Forecast of Local Lake-Effect Snowfall: The Case of Buffalo, U.S.A. *Int. J. Environ. Res.*, **7**, 859-868.

Helmus, J. J. and S. M. Collis, 2016: The Python ARM Radar Toolkit (Py-ART), a Library for Working with Weather Radar Data in the Python Programming Language. *J. of Open Research Software*, **4**, 25.

Herzmann, D. E., 2020: Mtarchive Bufkit Archive. Iowa State University, accessed 11 April 2020, https://mtarchive.geol.iastate.edu/.

Hitchcock, J., 2019: Composite Analog Charts for Lake Effect Snowstorms on the Lower Great Lakes. *10th Great Lakes Atmos. Sci. Symp.*, Oswego, NY, Oswego State Chapter of the Amer. Meteor. Soc.

Humphreys, C.J., J. R. Klein, 2019: Determining Biases in Snowfall Forecasts for Ontario Lake-Effect Snow Events Using GIS Compositing. *10th Great Lakes Atmos. Sci. Symp.*, Oswego, NY, Oswego State Chapter of the Amer. Meteor. Soc.

Kessler, J., 2020: Great Lakes Ice Cover Database. NOAA Great Lakes Environmental Research Laboratory, accessed 17 April 2020, https://www.glerl.noaa.gov/data/ice/#historical.

Mahoney, E. A., and T. A. Niziol, 1997: BUFKIT: A software application toolkit for predicting lake effect snow. Preprints, *13th International Conf. on Interactive Information and Processing Systems (IIPS) for Meteorology, Oceanography, and Hydrology*, Long Beach, CA, Amer. Meteor. Soc., 388–391.

May, R. M., S. C. Arms, P. Marsh, E. Bruning, J. R. Leeman, K. Goebbert, J. E. Thielen, and Z. Bruick, 2020: MetPy: A Python Package for Meteorological Data. Version 1.0.0rc1, Unidata, Accessed 14 January 2020.

Niziol, T. A., 1987: Operational Forecasting of Lake Effect Snowfall in Western and Central New York. *Wea. Forecasting*, **2**, 310-321.

Niziol, T. A., W. R. Snyder, and J. S. Waldstreicher, 1995: Winter Weather Forecasting throughout the Eastern United States. Part IV: Lake Effect Snow. *Wea. Forecasting*, **10**, 61–77.

Pedregosa, F. and coauthors, 2011: Scikit-learn: Machine Learning in Python. *J. of Machine Learning Research*. **12**. 2825–2830.

Steiger, S. M., R. Schrom, A. Stamm, D. Ruth, K. Jaszka, T. Kress, B. Rathbun, J. Frame, J. Wurman, and K. Kosiba, 2013: Circulations, bounded weak echo regions, and horizontal vortices observed within long lake-axis-parallel-lake-effect storms by the Doppler on Wheels. *Mon. Wea. Rev.*, **141**, 2821-2840.

Villani, J. P., M. L. Jurewicz, and K. Reinhold, 2017: Forecasting the Inland Extent of Lake Effect Snow Bands Downwind of Lake Ontario. *J. Operational Meteor.*, **5**, 53–70.

Watling, R., Guiney, J., 2015: Winter Weather Watch/Warning/Advisory Policy, Procedures, and Thresholds. National Weather Service Eastern Region Supplement ERS 02-2003, 13 pp, https://www.nws.noaa.gov/directives/sym/pd01005013e022003curr.pdf.